Strong superconductivity-induced phonon self-energy effects in $HgBa_2Ca_3Cu_4O_{10+\delta}$

V. G. Hadjiev, Xingjiang Zhou,* T. Strohm, and M. Cardona
Max-Planck-Institut für Festkörperforschung, Heisenbergstraße 1, D-70569 Stuttgart, Germany

Q. M. Lin and C. W. Chu
Department of Physics and the Texas Center for Superconductivity at the University of Houston, Houston, Texas 77204-5932
(Received 22 August 1997; revised manuscript received 1 December 1997)

We report strong superconductivity-induced phonon renormalization effects observed in the $HgBa_2Ca_3Cu_4O_{10+\delta}$ superconductor ($T_c = 123$ K). At the transition from the normal to the superconducting state, the A_{1g} phonons at 240 and 390 cm^{-1}, which correspond to vibrations of the plane oxygen atoms with some admixture of calcium vibrations, display an abrupt softening, and increase in linewidth within a rather narrow temperature interval. The changes of phonon self-energy are accompanied by a strong enhancement of the Raman intensity of the phonons in the superconducting state. The A_{1g} Raman peak at 575 cm^{-1}, related to the apex oxygen, and that at 487 cm^{-1} (tentatively attributed to excess oxygen) are not detectable in the normal state for incident light polarization in the ab plane. They, however, show up in the superconducting state as coupled phonon-electron excitations. To our knowledge, such phonon self-energy effects are the strongest ones reported for the superconducting cuprates so far. [S0163-1829(98)07725-X]

I. INTRODUCTION

Raman scattering of light by optical phonons in solids essentially proceeds via electron-phonon interactions. Those phonons, which are strongly coupled to electrons occupying states near the Fermi surface (FS), can be very sensitive to changes in the vicinity of the FS. In superconductors, the opening of the superconducting gap results in a redistribution of electronic states and excitations in the immediate vicinity of the FS which in turn changes the phonon self-energy, i.e., the contribution of the electron-phonon interaction to the phonon frequency and its linewidth. Superconductivity-induced phonon self-energy effects have been observed for a number of cuprates[1–6] and theoretically studied for the case of s-wave[7] and d-wave[8,9] superconductors. In particular, sizable effects have been observed for the B_{1g} out-of-phase plane oxygen phonon in $YBa_2Cu_3O_{7-\delta}$ (Y-123)[1,3,4] and for the A_{1g} phonons in $HgBa_2Ca_2Cu_3O_{8+\delta}$ (Hg-1223).[6] In addition, the appearance of a superconducting gap in the low-energy electronic excitations may also lead to resonancelike phenomena, e.g., increases in the Raman intensity of some phonons below the transition temperature T_c. Such increases have been seen in Y-123,[10] $YBa_2Cu_4O_8$ (Y-124),[11] and Hg-1223.[6] Experimentally measured superconductivity-induced changes in phonon frequencies and linewidths, in conjunction with model calculations,[7] have been used to estimate the magnitude of the superconducting gap in R-123 (R is a rare earth element).[3] Information on the superconducting order parameter can also be inferred from the electronic peak that develops below T_c due to quasiparticle creation through pair breaking,[12,13] provided the peak is discernible. Similarities of model calculations of the phonon self-energy and the electronic Raman efficiency,[14] with specific reference to d-wave paired superconductors, have been pointed out in Ref. 15: at low frequencies, the imaginary part of the phonon self-energy of *tetragonal* superconductors varies with frequency as ω^3 for the B_{1g} and as ω for A_{1g} spectra. Note, however, that in R-123 the B_{1g} and A_{1g} symmetries are mixed.[16]

In this paper, we report a collosal superconductivity-induced phonon self-energy effect which we have discovered in microcrystalline $HgBa_2Ca_3Cu_4O_{10+\delta}$ (Hg-1234) superconductors. We have observed a remarkable frequency softening and a linewidth increase of vibrations along the c axis involving the plane oxygen atoms with some admixture of calcium in a narrow temperature interval immediately below T_c, accompanied by a strikingly strong phonon intensity enhancement throughout the superconducting state. While rather elaborate theories exist for the self-energy effects of phonon frequencies and linewidths,[7,8] the corresponding effect on Raman intensities does not seem to have been theoretically treated. Moreover, the existing theories for the self-energy of phonons have so far not allowed the extraction of quantitative data on parameters relevant to the superconductivity from the available experimental results. We thus propose a simple quantum mechanical scheme which allows us to relate the enhancement of the Raman intensities observed in the superconducting state to the real part of the corresponding self-energy and to obtain semiquantitative information on the corresponding electron-phonon coupling constant.

II. EXPERIMENT

We measured single crystalline grains of Hg-1234 in a microcrystalline pellet ($T_c = 123$ K, determined by the zero of resistance) prepared by a high-pressure technique.[17] X-ray diffraction analysis confirmed that Hg-1234 was the main phase in the pellet. During the measurements the samples were kept in a continuous-flow liquid helium cryostat which was used to vary their temperature from 3.8 to 300 K. Raman spectra were excited with the 647.1 nm line of a Kr^+ laser and collected by a microprobe attachment of a Dilor XY spectrometer in an exact back-scattering geometry. The laser

power was kept low enough so that overheating amounted to no more than 5–10 K.

The compound Hg-1234, with four CuO_2 planes per primitive cell, crystallizes in the tetragonal $P4/mmm$ space group.[18] The group-theoretical analysis of the normal modes at the Γ point in Hg-1234 shows that $7A_{1g}$, $2B_{1g}$, and $9E_g$ modes are Raman allowed.[19] From the atomic site symmetries[20] in Hg-1234 it follows that the Ba atoms, those Ca atoms which are not at a center of inversion, the Cu atoms in the CuO_2 planes, and the apex oxygen can take part in the $A_{1g}+E_g$ modes. The oxygen atoms in the inner and outer pairs of CuO_2 planes contribute to the $A_{1g}+B_{1g}+2E_g$ modes. Based on the connection between the external morphology of the superconducting Hg-based cuprate crystals and the crystallographic axes,[6,19] we were able to choose crystals which allowed us to perform experiments in the $z(x'x')\bar{z}$, $z(x'y')\bar{z}$, and $x(zz)\bar{x}$ polarization configurations [written in Porto's notation $i(kl)j$, where i and j are the direction of propagation of the incident and scattered photons and k, l their polarization, respectively]. In this case z is parallel to the c axis of the crystal and x' and y' are two mutually orthogonal directions along $[110]$ and $[1\bar{1}0]$. For convenience, we give from now on only the polarization directions (pair of letters inside the parentheses in Porto's notation). Thus $x'x'$, $x'y'$, and zz configurations select the $A_{1g}+B_{2g}$, B_{1g}, and A_{1g} symmetry components of the Raman scattering tensor, respectively.

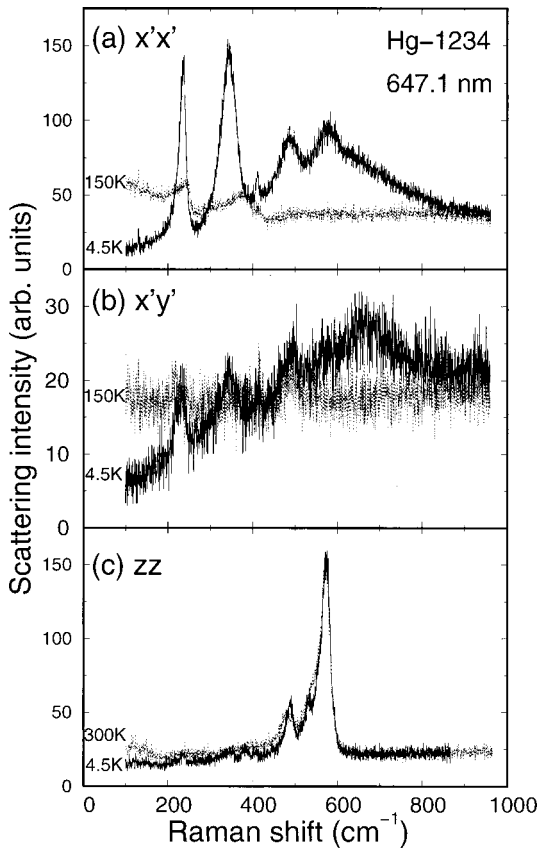

FIG. 1. Polarized Raman spectra of Hg-1234 single crystalline grains measured at room temperature (RT) and at 4.5 K with 647.1 nm laser excitation. The spectra (a) and (b) were taken from the same grain whereas those in (c) were measured from another grain oriented with the ac plane normal to the incident light.

III. EXPERIMENTAL RESULTS

In Fig. 1 we present polarized Raman spectra of Hg-1234 at room temperature and at 4.5 K. The spectra were recorded in those scattering geometries which select the most informative components of the Raman efficiency, namely, (a) $A_{1g}+B_{2g}$ $(x'x')$, (b) B_{1g} $(x'y')$, and (c) A_{1g} (zz). Only three clear Raman peaks at 574, 532, and 487 cm^{-1} are observable in the room temperature zz-polarized spectrum in Fig. 1(c). They become better resolved at low temperature. The strong peaks at 574, 532, and 487 cm^{-1} have been assigned to vibrations of the apex oxygen along the c axis and to mixed modes of apex and excess oxygen at different positions in the Hg plane.[19] Although of A_{1g} symmetry, these peaks do not appear in the $x'x'$ room temperature spectrum in Fig. 1(a) (note that there are no symmetry-allowed B_{2g} phonons). For this polarization configuration, and at room temperature, three weak phonon peaks are observable at 240, 390, and 410 cm^{-1}. The phonons at 240 and 390 cm^{-1} exhibit coupling with the scattering continuum manifested by an asymmetric line shape (Fano profile). The peak at 410 cm^{-1} has a symmetric profile and very low intensity. At low temperature, in the superconducting state, the two lower frequency phonons show an obvious change of their position, linewidth, and especially the scattering intensity. Except for an increase in intensity, there is no dramatic change of the 410 cm^{-1} phonon self-energy. In addition to these effects, two relatively sharp Raman features show up at 486 and 575 cm^{-1} on the top of the $A_{1g}+B_{2g}$ superconductivity-induced electronic peak [Fig. 1(a)]. Comparing with the spectra given in Fig. 1(c), one finds that the position of these peaks *correlates* with that of the mainly zz-polarized vibrations of the excess and apex oxygen atoms. Note that this is not because of polarization leakage. The line shape of the 574 cm^{-1} phonon in zz polarization is almost independent of temperature while the 575 cm^{-1} peak in the $x'x'$ spectra only exists in the superconducting phase. The two phonons of B_{1g} symmetry which are predicted by group theory are hardly seen in the room temperature spectrum of Fig. 1(b). Except for some Raman features that coincide in position with the peaks in the $x'x'$ spectra, likely due to polarization leakage, a relatively broad peak appears at 690 cm^{-1} that can be attributed to superconductivity-induced B_{1g} excitations of electronic origin. From now on we focus on the A_{1g} spectra.

We discuss next the assignment of the A_{1g} phonons at 240, 390, and 410 cm^{-1}. The symmetry and frequency of these phonons suggest that they involve vibrations along the c axis of plane oxygen atoms and of the Ca: the vibrations of Ba and Cu in the planes usually have frequencies below 200 cm^{-1} in the structurally similar superconducting cuprates; the A_{1g} apex oxygen vibration is seen at 574 cm^{-1} [Fig. 1(c)]. Since Ca has the lightest mass among the cations in Hg-1234, its frequency is expected to be close to that of the low frequency (bond bending) oxygen vibrations and the Ca vibrations may therefore mix with the latter. This gives a total of three Raman active A_{1g} modes in the 200–450 cm^{-1} region involving pairs of planes. Lattice dynamical calculations for the isomorphic Tl-1234 compound[21] indeed show

that the vibrations of Ca and plane oxygen atoms are mixed. In Ref. 21, it was calculated for Tl-1234 that the frequencies of the mixed vibrations along the c axis of oxygen in the CuO_2 planes and Ca moving in-phase and out-of-phase with the oxygen atoms are 246 and 450 cm^{-1}, respectively. One phonon corresponds nearly exclusively to the vibration against each other of the two CuO_2 layers which are separated by Ca atoms. This phonon has a small admixture of calcium and should be found at 369 cm^{-1}. Unfortunately, there are no experimental data available so far for Tl-1234 that may check the lattice dynamical predictions, while the calculations just mentioned, based on semiempirical lattice dynamical models, are known to be rather unreliable, especially concerning eigenvectors.[22] *Ab initio* calculations, based on the electronic total energy,[23,24] would be highly desirable in order to achieve a more reliable assignment of the frequencies and eigenvectors of the three A_{1g} modes under discussion. Nevertheless even these calculations are known to lead to considerable errors in the phonon eigenvectors, especially when phonon frequencies corresponding to the same symmetry are close to each other. A way to solve this problem is to determine the eigenvectors experimentally by isotopic substitution,[22] an investigation which has not yet been performed for the Hg-based superconductors. As a possible way out of the impass discussed above we examine the possibility of adopting the eigenvalues and eigenvectors calculated for Tl-1234 for the interpretation of our data concerning the 240, 390, and 410 cm^{-1} phonons of Hg-1234. The similarity of the electron-phonon coupling strength of the modes at 240 and 390 cm^{-1}, as displayed by their lineshape and dependence of Raman intensity on temperature, suggests that these two phonons should have some common vibrational patterns. In addition, the phonons at 265 and 400 cm^{-1} in Hg-1223 have similar temperature dependence as those at 240 and 390 cm^{-1} in Hg-1234.[6] In the Hg-1223 compound there are only two Raman active mixed plane-oxygen and Ca modes.[21] Therefore, we assign the A_{1g} modes at 240 and 390 cm^{-1} in Hg-1234 to the mixed Ca and oxygen modes and that at 410 cm^{-1} to pure plane oxygen vibrations along the c axis. The weak electron-phonon coupling observed for the 410 cm^{-1} phonon would then have to result from some cancellation within each pair of CuO_2 planes sandwiching the Ca plane, possibly related to the fact that those CuO_2 planes move in opposite direction.

Figure 2 shows the temperature evolution of the A_{1g} phonon modes of Hg-1234 as measured in the $x'x'$ configuration. The 240 and 390 cm^{-1} phonon lines display clear asymmetric line shapes with a characteristic antiresonance at the higher frequency side in the whole range from room temperature to 4.5 K, a fact which suggest an interaction between discrete (phonon) states and a broad (electronic) continuum, as found for other cuprates.[1,3,6] We have fitted the measured phonon lines with a standard Fano function[25]

$$I(\omega)=I_c\frac{|q+\epsilon|^2}{1+\epsilon^2}+I_b(\omega), \tag{1}$$

in which $\epsilon=(\omega-\omega_p)/\Gamma_p$ with the renormalized phonon frequency $\omega_p=\omega_p^0+\delta\omega_p$, ω_p^0 is the ''bare'' phonon frequency, q the asymmetry parameter, Γ_p the linewidth [given as half width at half maximum (HWHM)], I_c a quantity proportional

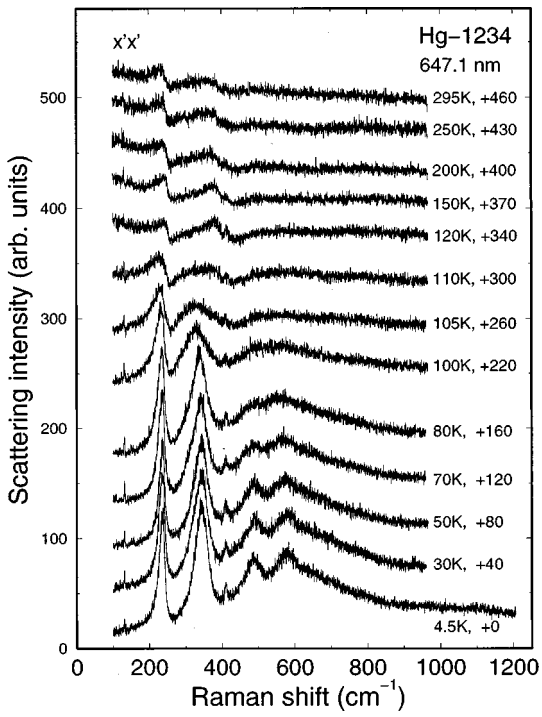

FIG. 2. Raman spectra of Hg-1234 measured at various temperatures between RT and 4.5 K in $x'x'$ polarization. The numbers in the right column give the offset of the spectra with respect to that at the bottom.

to the square of the Raman vertex of that part of the electronic continuum that interferes with the phonon, and $I_b(\omega)$ is the spectral function of a noninterfering background. Raman spectra and the fitted Fano profiles of the 240 and 390 cm^{-1} phonons are shown in Figs. 3(a) and 4(a), respectively. The fitted values of the Fano parameters (except for the trivial background I_b) and the *renormalized phonon intensity*[26]

$$I_p\equiv\pi[I(\omega_p)-I_b(\omega_p)]\Gamma_p=\pi I_c q^2\Gamma_p \tag{2}$$

of the 240 and 390 cm^{-1} peaks are plotted vs temperature in Figs. 3(b) and 4(b). (We assume that q is real. An imaginary part of q can be represented by a noninteracting electronic background, i.e., by I_b, see Ref. 25.) Note that I_c and I_b are intensities per unit frequency while I_p is the *integrated* intensity of the discrete phonon excitation.

Apart from some differences in details, the temperature dependences of frequency, linewidth, and intensity of the 240 and 390 cm^{-1} peaks display a remarkable abrupt change in a narrow temperature interval (10–15 K) right below T_c. Using the phonon frequencies ω_p^N and ω_p^S in the normal state and in the superconducting state, the relative softening $(\omega_p^N-\omega_p^S)/\omega_p^N$ of the 240 and 390 cm^{-1} phonons is 6 and 18%, respectively. Simultaneously, the phonon linewidth goes through a maximum below T_c with an overall change in linewidths $(\delta\Gamma_p)_{\max}/\omega_p^N$ equal to 10% for the phonon at 240 cm^{-1} and 40% for that at 390 cm^{-1}.

In the normal state, the linewidths of the 240 and 390 cm^{-1} phonons increase with increasing temperature. This indicates that at least two types of decay channels contribute to the phonon linewidth. The temperature-dependent channel

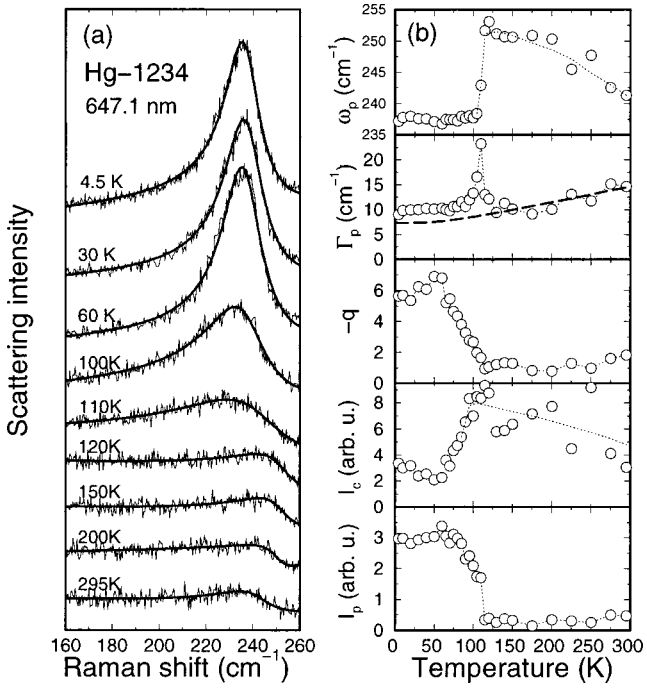

FIG. 3. Raman spectra of the A_{1g} mode at 240 cm^{-1} measured in $x'x'$ polarization with the 647.1 nm laser line at different temperatures and the corresponding fitted Fano profiles (a). The fitted frequency, linewidth Γ_p (HWHM), asymmetry parameter q, and the phonon intensity are plotted in (b) as open circles. Smooth dotted lines are given as a guide to the eye. The dashed line in the linewidth panel represents a fit to the widths found above T_c with the function in Eq. (2), taking $\omega_p = 240$ cm^{-1}. This fit yields $\Gamma^0_{\rm anh} = 3$ cm^{-1} and $\Gamma_b = 4.4$ cm^{-1}.

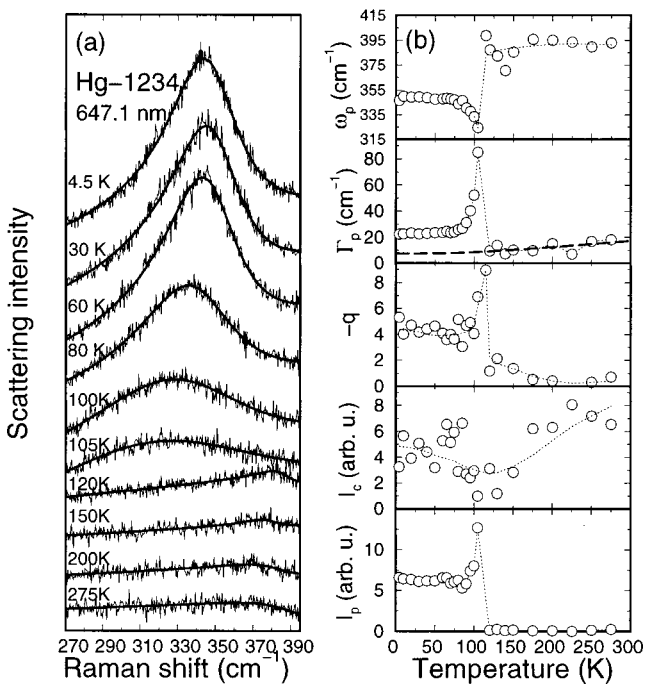

FIG. 4. Raman spectra covering the 390 cm^{-1} A_{1g} mode measured in $x'x'$ polarization with the 647.1 nm laser line at different temperatures and the corresponding fits with Fano profiles (a). The fitted frequencies, linewidths Γ_0 (HWHM), line shape parameters q, and the phonon intensity are represented in (b) by open circles. Smooth dotted lines are given as a guide to the eye. The dashed line in the linewidth panel represents a fit to the widths found above T_c with the function in Eq. (2), taking $\omega_p = 390$ cm^{-1}. This fit yields $\Gamma^0_{\rm anh} = 7.3$ cm^{-1}.

can be described in many solids by anharmonic decay[27] of the phonon with frequency ω_p and zero wave vector into two phonons with opposite wave vectors and frequencies close to $\omega_p/2$. This implies $\Gamma_{\rm anh}(T) = \Gamma^0_{\rm anh}[1 + 2n_B(\omega_p/2)]$, where n_B is the Bose-Einstein factor. An additional nearly temperature-independent contribution Γ_b to the linewidth may result from phonon scattering by impurities and, in the normal state, to the coupling of the phonon to the continuum of electronic excitations. We have fitted the temperature dependence of the phonon linewidths $\Gamma_p(T)$ at 240 cm^{-1} [Fig. 3(b)] and 390 cm^{-1} [Fig. 4(b)] in the normal state using the function

$$\Gamma^N_p(T) = \Gamma^0_{\rm anh}\left(1 + \frac{2}{\exp(\hbar\omega_p/2k_BT) - 1}\right) + \Gamma_b . \qquad (3)$$

Note that $\Gamma^N_p(T=0) = \Gamma^0_{\rm anh} + \Gamma_b$ is the sum of the temperature-dependent part of $\Gamma^N_p(T)$ at $T=0$ and the temperature-independent part Γ_b. Consequently, the *change* in linewidth due to the superconducting transition is given by the linewidth at $T=0$ minus $\Gamma^N_p(T=0)$, i.e., $\delta\Gamma_p = \Gamma_p(0) - (\Gamma^0_{\rm anh} + \Gamma_b)$. The dashed line in Fig. 3(b) represents the fit with Eq. (3) (linewidths are given as HWHM) with $\Gamma^0_{\rm anh} = 3$ cm^{-1} and $\Gamma_b = 4.4$ cm^{-1} taking $\omega_p = 240$ cm^{-1} (these quantities have rather large error bars). The fit allows us to distinguish between the temperature-dependent contribution $\Gamma_{\rm anh}$, and the constant contribution Γ_b to the linewidth, of which the latter is likely to be due to the interaction of the 240 cm^{-1} phonon with electronic excitations in the normal state and/or impurity scattering. The fit of the temperature dependence of the 390 cm^{-1} phonon linewidth with Eq. (3) yields $\Gamma_b \approx 0$. The results of such a fit are represented by the dashed line in Fig. 4(b). The fitting parameters for this case are $\Gamma^0_{\rm anh} = 7.3$ cm^{-1} for $\omega_p = 390$ cm^{-1}. The strongest change in the phonon linewidth takes place just below T_c, as would be expected for a crossover of the opening superconducting gap and the phonon energy. When further lowering the temperature the linewidth remains nearly constant.

IV. DISCUSSION

The expression in Eq. (1) for the Raman efficiency of a system with a phonon coupled to a continuum of excitations (here we consider electronic excitations) can be written in terms of microscopic parameters[28,29] (neglecting for simplicity other phonon renormalization mechanisms as, for instance, anharmonic decay)

$$I(\omega) \sim \pi T_e^2 \rho(\omega) \frac{(\omega - \omega_p^0 + T_p V/T_e)^2}{[\omega - \omega_p^0 - V^2 R(\omega)]^2 + [\pi V^2 \rho(\omega)]^2}, \qquad (4)$$

where T_e, T_p, and V are the vertices describing the coupling of the electron-hole excitations to the photons (Raman vertex), the coupling of the phonons to the photons, and the electron-phonon coupling, respectively. The bare phonon

frequency is ω_p^0. The continuum spectral function $\rho(\omega)$ and the function $R(\omega)$ are related to the imaginary and the real part of the retarded electronic polarizability $\Pi(\omega)$ at $\mathbf{q}=0$ by

$$\rho(\omega)=-\frac{1}{\pi}\mathrm{Im}\ \Pi(\omega) \quad \text{and} \quad R(\omega)=\mathrm{Re}\ \Pi(\omega), \tag{5}$$

respectively. A Kramers-Kronig relation allows us to calculate $R(\omega)$ from $\rho(\omega)$. Note that $\rho(\omega)$ is an odd function of ω, this is a general property of retarded correlation functions and has to be kept in mind when performing the Kramers-Kronig transformation.

In Eq. (4), it is implicitly assumed that the vertices T_e, T_p, and V are all independent of energy and momentum and are real. These assumptions are justified by the small range of energies covered by the Raman spectra. We will also assume that the vertices T_e and T_p do not change much when crossing the superconducting phase transition at $T=T_c$. These Raman vertices include electronic transitions to intermediate states (with $\mathbf{k}$ conservation) which may have energies close to those of laser photons ω_L. The band structure changes at T_c only in a region of width approximately twice the maximum gap $2\Delta_0$ around the Fermi energy. Therefore, and because of the fact that $2\Delta_0$ is considerably less than the typical lifetime broadening of interband transitions, the resonance conditions should not change much upon crossing T_c. Hence, the Raman vertex T_e can be assumed to be the same in the normal as in the superconducting state. This assumption has received ample confirmation in the cases of Y-123 (Ref. 30) and Y-124.[13,31] The vertex T_p involves first absorbing a photon, then emitting a phonon and after that emitting the scattered photon. Also in this case, and for the same reasons, it is unlikely that T_p would change when crossing T_c.

We conclude from Eq. (4) that the broadening of the phonon due to the coupling to the continuum of excitations is given by[3]

$$\Gamma=\pi V^2\rho(\omega_p). \tag{6}$$

Note that anharmonic broadening Γ_{anh} can be included by replacing $\pi V^2\rho(\omega)$ in Eq. (4) by $\pi V^2\rho(\omega)+\Gamma_{\mathrm{anh}}$ provided the real part of the self energy $\delta\omega_p^{\mathrm{anh}}$ given by anharmonic broadening does not vary much around ω_p^0. In this case $\delta\omega_p^{\mathrm{anh}}$ can be absorbed as a frequency shift into ω_p^0 [i.e., we replace $\omega_p^0+\delta\omega_p^{\mathrm{anh}}(\omega_p^0)$ by ω_p^0 in Eq. (4)].

If we attempt to determine V by fitting experimental data with Eq. (6), we are faced with a problem. When trying to calculate V from the linewidth, we need to know the electron spectral function $\rho(\omega)$. In the case of vanishing electron-phonon coupling V, Eq. (4) gives $I(\omega)\sim\pi T_e^2\rho(\omega)$. Although T_e is unknown it can be taken as a scaling factor when we represent the data in arbitrary units. On the other hand, from the theory of electronic Raman scattering in the superconducting state, we know that for tetragonal superconductors with a gap function of $k_x^2-k_y^2$ symmetry (B_{1g} in the D_{4h} point group) the function $\rho(\omega)$ is linear in ω in the low-frequency regime ($\omega\lesssim\Delta_0$) (Refs. 13,15). Under this assumption and using Eq. (6), we can calculate the ratio of the electron-phonon coupling constants for the two particular phonons at 390 and at 240 cm^{-1} *in the superconducting state* to be given by

$$\frac{V_{390}^2}{V_{240}^2}=\frac{\Gamma_{390}}{\Gamma_{240}}\frac{240\ \mathrm{cm}^{-1}}{390\ \mathrm{cm}^{-1}} \tag{7}$$

which yields $V_{390}/V_{240}\approx 1.5$.

The second possibility to obtain information about V from experimental spectra makes use of the frequency shift $\delta\omega_p=-V^2R(\omega_p)$. For this purpose we must know the unrenormalized energy which is, in principle, not an observable.

This problem can be overcome through the kindness of nature: in the material at hand the experimental data for the normal state suggest that V, and thus the phonon self-energy, is rather small. Nearly negligible electronic self-energy contributions to Γ_p in the normal state can be inferred from Figs. 3(b) and 4(b). The increase in Γ observed below T_c, in spite of the decrease in the electronic continuum at frequencies below $\approx 400\ \mathrm{cm}^{-1}$, also confirms the fact that V in the superconducting state is much larger than in the normal state. We shall make use of this fact to obtain the real and imaginary parts of the self energy in the superconducting state by referring the corresponding frequencies and widths to those in the normal state (which are assumed to vanish). The reason why V in the normal state differs from that in the superconducting state can be attributed to the different types of averages of the electron-phonon matrix elements $g_{\mathbf{k}}$ which are relevant to the two cases. For the normal state we have

$$V^2\sim\langle g_{\mathbf{k}}^2\rangle_{\mathrm{FS}}-\langle g_{\mathbf{k}}\rangle_{\mathrm{FS}}^2, \tag{8}$$

where $\langle\cdots\rangle_{\mathrm{FS}}$ represents an average over the four sheets of the Fermi surface and $\langle g_{\mathbf{k}}\rangle_{\mathrm{FS}}^2$ corresponds to the electrostatic screening required for A_{1g} phonon modes.[15] Note that if $g_{\mathbf{k}}$ is constant over the four Fermi surface sheets, V^2 vanishes due to screening (this only happens for phonons with the full symmetry of the point group, i.e., A_{1g} in the D_{4h} case, otherwise $\langle g_{\mathbf{k}}\rangle_{\mathrm{FS}}$ vanishes while $\langle g_{\mathbf{k}}^2\rangle_{\mathrm{FS}}$ does not).

In the superconducting state, Eq. (8) must be replaced by

$$V^2\sim\langle g_{\mathbf{k}}^2\lambda_{\mathbf{k}}(\omega)\rangle_{\mathrm{FS}}-\frac{\langle g_{\mathbf{k}}\lambda_{\mathbf{k}}(\omega)\rangle_{\mathrm{FS}}^2}{\langle\lambda_{\mathbf{k}}(\omega)\rangle_{\mathrm{FS}}}, \tag{9}$$

where $\lambda_{\mathbf{k}}(\omega)$ is the Tsuneto function.[12,13] If $\lambda_{\mathbf{k}}$ is not constant over the Fermi surface sheets, the averages in Eqs. (8) and (9) can be rather different, a fact which allows for the near vanishing of Eq. (8) suggested by the experimental data.

We note, however, that values of the Fano parameter q of the order of one are found for the two phonons in the normal state. Correspondingly, sigmoid-type spectra can be seen for these phonons in Fig. 2 in spite of their meager strength. The expression for q is [see Eqs. (1) and (4)]

$$q=\frac{VT_p/T_e+V^2R(\omega)}{\pi V^2\rho(\omega)}. \tag{10}$$

The weak phonon spectra observed in the normal state allow us to set $T_p\approx 0$. The values of $q\approx 1$ found experimentally thus imply that $R\approx\rho$.

We consider next the large frequency shifts $\delta\omega_p$ and the increase in the phonon intensity observed when lowering T

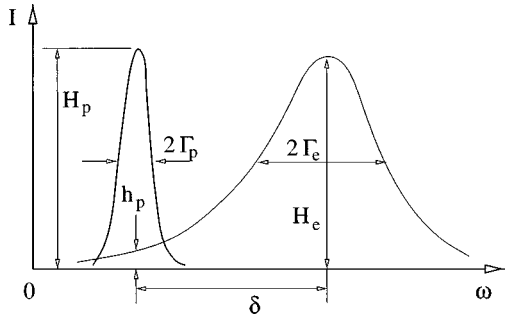

FIG. 5. Definition of quantities used in the text for the electronic and phonon spectra of Hg-1234.

below T_c. In view of the many uncertainties involved in detailed microscopic theories (which are not meant to apply to the case of four CuO_2 layers anyhow) we propose a simple treatment which is physically transparent and yields results in reasonable agreement with the observations. The calculations are based on the schematic representation of the electronic scattering spectra shown in Fig. 5. Instead of performing the Kramers-Kronig integrations required for the calculation of $\delta\omega_p$ we replace the electronic spectrum of Fig. 5 by a δ function at its maximum. This yields

$$\delta\omega_p = -V^2 R(\omega_p) = -(\Gamma_p - \Gamma^0_{\rm anh})\frac{R(\omega_p)}{\pi\rho(\omega_p)}. \qquad (11)$$

Because of the fact that $R(\omega)$ and $\rho(\omega)$ are related by a Kramers-Kronig transform, we can express the quotient on the right side of Eq. (11) as $-H_e\Gamma_e/(h_p\delta)$, where the parameters are defined in Fig. 5. Then, the line shift can be written as

$$\delta\omega_p = \frac{H_e}{h_p}\frac{\Gamma_e(\Gamma_p - \Gamma^0_{\rm anh})}{\delta}. \qquad (12)$$

For the phonons at 240 and 390 cm^{-1} we use this relation to calculate ''theoretical'' line shifts $\delta\omega_p^{\rm theo}$ and compare these to the experimentally determined line shifts $\delta\omega_p^{\rm exp}$. The results are given in Table I. In the case of the 487 and 575 cm^{-1} phonons, the line shift cannot be meaningfully determined from the experiment.

A similar expression can be derived for the height of the phonon peak H_p. We start with Eq. (2) and use $q\Gamma_p = \delta\omega_p$ as well as $q = R(\omega_p)/[\pi\rho(\omega_p)]$. This yields

$$I_p = \frac{I_c}{\pi T_e^2 \rho(\omega_p)}\pi T_e^2 R(\omega_p)\delta\omega_p. \qquad (13)$$

The quotient on the right side of this relation is one, and the factor $\pi T_e^2 R(\omega_p)$ is the Kramers-Kronig transform of the electronic Raman intensity at $\omega = \omega_p$. In suitable units we write $I_p = \pi H_p \Gamma_p$ and $\pi T_e^2 R(\omega_p) = \pi H_e \Gamma_e/\delta$ and get for the ratio of the phonon height to the height of the electronic peak the relation

$$\frac{H_p}{H_e} = \frac{\Gamma_e}{\Gamma_p}\frac{\delta\omega_p}{\delta}. \qquad (14)$$

We use this relation to calculate ''theoretical'' phonon heights $H_p^{\rm theo}$ of the 240 and 390 cm^{-1} phonons and compare them to the experimentally determined phonon heights $H_p^{\rm exp}$ in Table I. For the 487 and 575 cm^{-1} phonons we use Eq. (14) to calculate the line shift which is experimentally not accessible.

The agreement of the ''theoretical'' values for the phonon lineshifts $\delta\omega_p^{\rm theo}$ and phonon heights $H_p^{\rm theo}$ and its experimentally determined counterparts $\delta\omega_p^{\rm exp}$ and $H_p^{\rm exp}$, respectively, is quite satisfactory, especially when one considers the simplicity of the theory.

For the purpose of extracting the coupling constant V from the experimental spectra, the Raman vertex T_e has to be known. Although it could be determined from experiment,[13] we will use here another approach to characterize the electron-phonon coupling strength. We define the number of electronic states N_e involved in the electronic peak around $\omega = \omega_e$ by $\rho(\omega) = N_e\delta(\omega - \omega_e)$. Then, Eq. (11) reads

$$N_e V^2 = \delta\omega_p \cdot \delta \qquad (15)$$

and can be used to determine the values of the combination $N_e V^2$ from the experiment (see Table I).

It is of interest to express the electron-phonon coupling strength by means of McMillan's electron-phonon interaction parameter λ which in Eliashberg's theory plays the role of the combination ''$N(0)V$'' in the BCS theory and also represents the mass enhancement of electrons $(1+\lambda)$ due to their coupling to the phonon system. This parameter is defined by[32]

TABLE I. The per-phonon quantities at $T=0$ used in the text. The electronic peak is characterized by its position $\omega_e = 620$ cm^{-1}, its linewidth $\Gamma_e = 250$ cm^{-1}, and its peak intensity $H_e = 80$ a.u. Here, a.u. denotes the arbitrary units for the intensities taken from Fig. 1. The line shift $\delta\omega_p^{\rm theo}$ and the phonon height $H_p^{\rm theo}$ are calculated using Eqs. (12) and (14), respectively, for the 240 and 390 cm^{-1} phonons. The line shift $\delta\omega_p^{\rm theo}$ of the 487 and 574 cm^{-1} phonons is as predicted by Eq. (14). The coupling strength $N_e V^2$ and electron-phonon coupling parameter λ_ν have been determined using Eq. (15) and Eq. (19), respectively, for all four phonons.

ω_p (cm^{-1})	Γ_p (cm^{-1})	$\Gamma^0_{\rm anh}$ (cm^{-1})	δ (cm^{-1})	h_p (a.u.)	$\delta\omega_p^{\rm theo}$ (cm^{-1})	$\delta\omega_p^{\rm exp}$ (cm^{-1})	$H_p^{\rm theo}$ a.u.	$H_p^{\rm theo}$ (cm^{-1})	$H_p^{\rm exp}$ a.u.	$H_p^{\rm exp}$ (cm^{-1})	$N_e V^2$ (cm^{-2})	λ_ν
240	9	3	380	20	16	15	87		120		5700	0.08
390	22	7.3	230	35	37	40	158		110		9200	0.08
487	23		133		6.1				40		810	5×10^{-3}
574	30		45		2.2				32		99	6×10^{-4}

$$\lambda = 2\int_0^\infty d\omega \frac{\alpha^2 F(\omega)}{\omega}, \tag{16}$$

where the spectral function $\alpha^2 F(\omega)$ determines the transition temperature T_c in Eliashberg's theory. Using the electronic density of states at the Fermi level $N_0 = 2\Sigma_{\mathbf{k}}\delta(\epsilon_{\mathbf{k}})$ in the normal state, $\alpha^2 F(\omega)$ is given by the expression[32]

$$\alpha^2 F(\omega) = N_0^{-1} \sum_{\nu,\mathbf{k}\sigma,\mathbf{k}'\sigma'} |V_{\nu,\mathbf{k}\sigma,\mathbf{k}'\sigma'}|^2 \delta(\omega - \omega_{\nu,\mathbf{k}-\mathbf{k}'}) \times \delta(\epsilon_{\mathbf{k}})\delta(\epsilon_{\mathbf{k}'}), \tag{17}$$

where $V_{\nu,\mathbf{k}\sigma,\mathbf{k}'\sigma'}$ is the electron-phonon matrix element for phonon branch ν, $\omega_{\nu,\mathbf{k}}$ is the frequency of the phonon of branch ν with momentum $\mathbf{k}$, and the sum over ν includes all optical phonons. Because of the fact that Raman scattering only gives information about phonons at the center of the BZ (Γ point), we approximate the optical phonons by dispersionless phonons with the frequency given by that of the corresponding Γ-point phonon, i.e., $\omega_{\nu,\mathbf{q}} = \omega_{\nu,\mathbf{q}=0} \equiv \omega_{p,\nu}$ and also take $V_{\nu,\mathbf{k}\sigma,\mathbf{k}'\sigma'} = V_\nu \delta_{\sigma\sigma'}$. Replacing Eq. (17) into Eq. (16) yields

$$\lambda = N_0 \sum_\nu \frac{V_\nu^2}{\omega_{p,\nu}}. \tag{18}$$

The λ represented by Eq. (18) is to be regarded as the contribution to λ which one would have if all phonons of a given branch would couple as much as that at the Γ point. We have determined above for several phonons values of $V^2 N_e$ where N_e is the total number of interacting excitations induced by the superconductivity. To a reasonable approximation we can write $N_e \approx \Delta_0 N_0$ and, therefore,

$$\lambda = \sum_\nu \lambda_\nu, \quad \lambda_\nu = \frac{1}{\Delta_0}\frac{N_e V_\nu^2}{\omega_{p,\nu}}. \tag{19}$$

Using $\Delta_0 = 310$ cm^{-1}, the values of λ_ν are given by 0.08, 0.08, 5×10^{-3}, and 6×10^{-4} for the phonons at 240, 390, 487, and 575 cm^{-1} respectively. In order to get a feeling for the magnitude of these electron-phonon coupling constants we note that if all phonons had the same value of λ_ν as that determined for the 390 cm^{-1} phonon (≈ 0.1), the total λ would be $0.1\times60 = 6$, a large value indeed which would lead to a very high T_c if taken literally in the BCS theory.

V. CONCLUSIONS

We have observed superconductivity-induced phonon self-energy effects for the A_{1g} phonons in Hg-1234 which show a strength exceeding that found in any other cuprate superconductors studied so far. The dramatic softening of the 240 and 390 cm^{-1} phonons below T_c is similar to that required to interpret the change in vibrational amplitude which has been observed in nearly optimally doped $YBa_2Cu_3O_{7-\delta}$ at T_c in ion channelling experiments[33] (see also the results from resonant neutron absorption spectroscopy in $Bi_2Sr_2CaCa_2O_8$, Ref. 34). The phonon self-energy effects, in combination with a clear development of the superconductivity-induced electronic Raman peaks, offers a unique opportunity for a detailed theoretical modeling of electron-phonon coupling processes in superconducting cuprates. In spite of the large values of λ associated with the large electron-phonon coupling effects discussed here, the question of a possible connection between the observed strong electron-phonon coupling and the remarkably high T_c of the Hg-based superconducting cuprates must remain open.

ACKNOWLEDGMENTS

We thank H. Hirt and M. Siemers for expert technical help, and V. Belitsky for numerous useful discussions and for a critical reading of the manuscript. X.J.Z. acknowledges the Alexander von Humboldt Foundation for financial support. This work was supported in part by NSF Grant No. DMR 95-10625, T. L. L. Temple Foundation, John J. and Rebecca Moores Endowment, and the State of Texas through the Texas Center for Superconductivity at the University of Houston.

*On leave from National Lab for Superconductivity, Institute of Physics, Chinese Academy of Sciences, Beijing 100080, China; present address: Advanced Light Source, LBNL, University of California, Berkeley, California 94720.

[1] S. L. Cooper, M. V. Klein, B. G. Pazol, J. P. Rice, and D. M. Ginsberg, Phys. Rev. B **37**, 5920 (1988).
[2] C. Thomsen, M. Cardona, B. Friedl, I. I. Mazin, O. Jepsen, O. K. Andersen, and M. Methfessel, Solid State Commun. **75**, 219 (1990).
[3] B. Friedl, C. Thomsen, and M. Cardona, Phys. Rev. Lett. **65**, 915 (1990).
[4] E. Altendorf, X. K. Chen, J. C. Irwin, R. Liang, and W. N. Hardy, Phys. Rev. B **47**, 8140 (1993).
[5] D. H. Leach, C. Thomsen, and M. Cardona, Solid State Commun. **88**, 457 (1993).
[6] X. J. Zhou, M. Cardona, D. Colson, and V. Viallet, Phys. Rev. B **55**, 12 770 (1997).
[7] R. Zeyher and G. Zwicknagl, Z. Phys. B **78**, 175 (1990).
[8] E. J. Nicol, C. Jiang, and J. P. Carbotte, Phys. Rev. B **47**, 8131 (1993).
[9] C. Jiang and J. P. Carbotte, Phys. Rev. B **50**, 9449 (1994).
[10] B. Friedl, C. Thomsen, H.-U. Habermeier, and M. Cardona, Solid State Commun. **81**, 989 (1992).
[11] E. T. Heyen, M. Cardona, J. Karpinski, E. Kaldis, S. Rusiecki, Phys. Rev. B **43**, 12 958 (1991).
[12] T. P. Devereaux, D. Einzel, B. Stadlober, and R. Hackl, Phys. Rev. Lett. **72**, 3291 (1995); T. P. Devereaux and D. Einzel, Phys. Rev. B **51**, 16 336 (1995).
[13] T. Strohm and M. Cardona, Phys. Rev. B **55**, 12 725 (1997).
[14] M. Cardona and I. P. Ipatova, in *Elementary Excitations in Solids*, edited by J. L. Birman, C. Sébenne, and R. F. Wallis (Elsevier, Amsterdam, 1992), p. 237.
[15] T. P. Devereaux, Phys. Rev. B **50**, 10 287 (1994); T. P. Devereaux and D. Einzel, *ibid.* **54**, 15 547 (1996).
[16] T. Strohm and M. Cardona, Solid State Commun. **104**, 223 (1997).
[17] Q. M. Lin, Z. H. He, Y. Y. Sun, L. Gao, Y. Y. Xue, and C. W. Chu, Physica C **254**, 207 (1995).
[18] E. V. Antipov, S. M. Loureiro, C. Chaillout, J. J. Capponi, P. Bordet, J. L. Tholence, S. N. Putilin, and M. Marezio, Physica C **215**, 1 (1993).

[19] X. J. Zhou, M. Cardona, C. W. Chu, Q. M. Lin, S. M. Loureiro, and M. Marezio, Physica C **270**, 193 (1996).
[20] D. L. Rousseau, R. P. Bauman, and S. P. S. Porto, J. Raman Spectrosc. **10**, 253 (1981).
[21] A. D. Kulkarni, F. W. de Wette, J. Prade, U. Schröder, and W. Kress, Phys. Rev. B **41**, 6409 (1990).
[22] R. Henn, T. Strach, E. Schrönherr, and M. Cardona, Phys. Rev. B **55**, 3285 (1997).
[23] C. O. Rodriguez, A. I. Liechtenstein, I. I. Mazin, O. Jepsen, O. K. Andersen, and M. Methfessel, Phys. Rev. B **42**, 2692 (1990).
[24] W. E. Pickett, R. E. Cohen, and H. Krakauer, Phys. Rev. B **42**, 8764 (1990).
[25] G. Abstreiter, M. Cardona, and A. Pinczuk, in *Light Scattering in Solids IV*, edited by M. Cardona and G. Güntherodt (Springer, Berlin, 1984), p. 128.
[26] M. Chandrasekhar, H. R. Chandrasekhar, M. Grimsditch, and M. Cardona, Phys. Rev. B **22**, 4825 (1980).
[27] J. Menéndez and M. Cardona, Phys. Rev. B **29**, 2051 (1984).
[28] M. V. Klein, in *Light Scattering in Solids I*, edited by M. Cardona (Springer, Berlin, 1983), p. 171f.
[29] V. I. Belitsky, A. Cantarero, M. Cardona, C. Trallero-Giner, and S. T. Pavlov, J. Phys.: Condens. Matter **9**, 5965 (1997).
[30] M. Krantz, Phys. Rev. B **54**, 1334 (1996).
[31] S. Donovan, J. Kircher, J. Karpinski, E. Kaldis, and M. Cardona, J. Supercond. **8**, 417 (1995).
[32] P. B. Allen, Phys. Rev. B **6**, 2577 (1972).
[33] R. P. Sharma, T. Venkatesan, Z. H. Zhang, J. R. Liu, R. Chu, and W. K. Chu, Phys. Rev. Lett. **77**, 4624 (1996).
[34] H. A. Mook, M. Mostoller, J. A. Harvey, N. W. Hill, B. C. Chakoumakos, and B. C. Sales, Phys. Rev. Lett. **65**, 2712 (1990).